Single-Event Effect Responses of Integrated Planar Inductors in 65-nm CMOS

Stefan Biereigel, Szymon Kulis, Paul Leroux, *Senior Member, IEEE*, Paulo Moreira, Alexander Kölpin, *Senior Member, IEEE*, and Jeffrey Prinzie, *Member, IEEE*

***Abstract*— This article describes a previously unreported single-event radiation effect in spiral inductors manufactured in a commercial CMOS technology when subjected to ionizing radiation. Inductors play a major role as the component determining the frequency of *LC* tank oscillators, which is why any radiation effect in these passive components can have a detrimental impact on the performance of clock generation circuits. Different experiments performed to localize and characterize the single-event effect (SEE) response in a radiation-hardened PLL circuit are discussed and presented together with a hypothesis for the underlying physical mechanism.**

***Index Terms*— Inductors, metal–insulator structures, oscillators, phase-locked loops (PLLs), radiation effects, SiO_2.**

I. Introduction

THE generation of high-quality reference clock signals is essential for many applications. One of the most common architectures to realize such synthesizers is phase-locked loop (PLL). Of special concern in radiation environments is the degradation of the reference signal quality that may lead to severe performance impairment and loss of functionality. Therefore, radiation hardening of PLLs is an important aspect for such circuits and systems. Due to their superior intrinsic phase noise performance compared to other topologies, PLLs often use integrated *LC* tank oscillators [1]. *LC* oscillator circuits have therefore undergone significant radiation-hardening efforts in recent years. These efforts have been focused on active devices, such as MOS transistors and varactors. Due to their well-known single-event effect (SEE) sensitivity [1]–[5] and total ionizing dose (TID) degradation [1], [6], [7], those components traditionally were the major contributors to radiation sensitivity in Voltage-Controlled Oscillators (VCOs). The *LC* tank itself, being composed of capacitors and an inductor, both passive components, was generally thought to be insensitive to ionizing radiation. As hardening efforts mature, performance requirements become more stringent, and the sensitivity of instrumentation used to detect radiation effects improves, this assumption appears to no longer hold: In this article, we describe the single-event radiation response originating in planar two-turn spiral inductor structures used to form the *LC* tank in high-performance oscillators. As another example, Xu *et al.* [8] have recently reported SEE responses generated in metal–oxide–metal capacitors in a 65-nm CMOS technology, another passive component crucial for the design of high-performance circuits.

Manuscript received August 30, 2021; revised October 4, 2021; accepted October 14, 2021. Date of publication October 18, 2021; date of current version November 18, 2021. This work was supported by the Wolfgang Gentner Programme of the German Federal Ministry of Education and Research under Grant 05E18CHA.

Stefan Biereigel is with CERN (European Center for Nuclear Research), 1211 Meyrin, Switzerland, also with the ESAT-ADVISE Research Laboratory, KU Leuven, 3000 Leuven, Belgium, and also with the Chair of Electronics and Sensor Systems, Brandenburg University of Technology, 03046 Cottbus, Germany (e-mail: stefan.biereigel@cern.ch).

Szymon Kulis and Paulo Moreira are with CERN (European Center for Nuclear Research), 1211 Meyrin, Switzerland.

Paul Leroux and Jeffrey Prinzie are with the ESAT-ADVISE Research Laboratory, KU Leuven, 3000 Leuven, Belgium.

Alexander Kölpin is with the Institute for High Frequency Technology, Hamburg University of Technology, 21073 Hamburg, Germany.

Color versions of one or more figures in this article are available at https://doi.org/10.1109/TNS.2021.3121029.

Digital Object Identifier 10.1109/TNS.2021.3121029

A. Single-Event Effects in LC PLLs

Conceptually, single-event effects in PLL synthesizers can be separated into two classes based on the mechanism disturbing the control loop. The first class of effects is phase discontinuities. Such discontinuities arise either when energy is directly injected into the tank [2] (e.g., through charge collection by the active devices of the oscillator) or when a memory element in the feedback divider is corrupted by single-event upset (SEU). Common to this class of effects is an abrupt change of output clock phase, which is followed by a recovery transient determined by the PLL dynamics. The second class of effects is frequency discontinuities. These occur when the oscillator frequency is altered, either by SEE affecting the VCO tuning node or any of the components determining the frequency (e.g., the inductance or capacitance forming the tank). Its transient response is characterized by a gradual buildup of phase error (for as long as the radiation effect altering the frequency persists), which is continuously counteracted by the feedback loop. This is a direct consequence of the VCO acting as an integrator, in this case, integrating a step frequency response to a linear ramp as its phase response. Radiation responses observed in PLL circuits may be a result of both these effects in superposition.

B. Organization of This Article

The main goal of this article is to describe the observed circuit responses in detail and indicate potential explanations for their origins and mechanism. Section II describes the circuit and its variants used in the irradiation experiments. In Section III, the experimental setup and methodology are presented. While Section IV reports on the results of the

This work is licensed under a Creative Commons Attribution 4.0 License. For more information, see https://creativecommons.org/licenses/by/4.0/

individual experiments, Section V contextualizes and links the individual experimental findings and explores different hypotheses for the origin of the observed responses.

II. Circuit Description

The measurements described in this article have been performed on a radiation-tolerant Integer-N PLL, which was previously presented in [9]. The VCO used in this circuit operates at 5.12 GHz and is locked to a reference clock of 40 MHz during the closed-loop operation. The *LC* tank is composed of a 930-pH inductor and a 1.04-pF capacitor. It is tuned using MOS varactors (in a radiation hardened configuration [10]), achieving a tuning sensitivity of 500 MHz V^{-1}. More details of the VCO implementation can be found in [11], which utilizes the same VCO as part of a clock and data recovery (CDR) circuit and expands further on the circuit-level SEE mitigation techniques implemented, especially with respect to the tuning topology. The loop filter includes a filter capacitor of 56pF and is designed for a loop bandwidth of 100 kHz. All digital circuit components (such as the phase–frequency detector and feedback divider) are protected by triple modular redundancy (TMR) against SEE. The analog blocks (charge pumps, loop filter, and VCO) are designed using state-of-the-art radiation-hardening techniques, including appropriate sizing and enclosed layout transistors to mitigate SEE and TID effects.

The circuit is designed and manufactured in a commercial 65-nm bulk CMOS technology with six metal layers. The two-turn spiral inductor, which will remain the focus of the following discussions, is implemented in the ultrathick top metal layer plus an underpass at a thick metal level just below. The copper metallization used for the inductor has a thickness of 3.5 μm and a width of 12 μm. The conductor is suspended on interlevel dielectrics at a height of about 4 μm above the silicon substrate. The two turns of the inductor are separated horizontally by a 3-μm gap, which is also filled with an insulating dielectric material. While the lower, thin metal layers in this process utilize low-κ dielectric materials to minimize interconnect parasitics, the upper level metals (which also makes up for the majority of vertical geometrical extent in our structure), to the best of our knowledge, utilize silicon dioxide, most likely deposited using chemical vapor deposition (CVD) methods. The inductor area is surrounded by a foundry-provided guard ring structure, which minimizes electrical coupling to adjacent structures and improves substrate noise isolation.

Two different versions of the inductor are used in the experiments described in the following. The version, henceforth referred to as "Inductor A," does not use any additional metal features in the area covered by the inductor, which implies that the inductor metal is separated from the silicon substrate only by dielectric layers. A modified version uses the same inductor geometry but includes a symmetrical patterned ground shield (PGS) on the lowest metal level just above the substrate. This ground shield is connected locally to the guard ring structure and the VCO circuit ground potential. The metal ground shield was included to significantly reduce electrical coupling between the substrate and the inductor while, at the same time, not influencing the electrical parameters (inductance and quality factor at the operating frequency) of the inductor itself [12]. This second version is referred to as "Inductor B." Both versions of the inductor geometry are shown side by side in Fig. 1, together with an approximate cross section of the geometry.

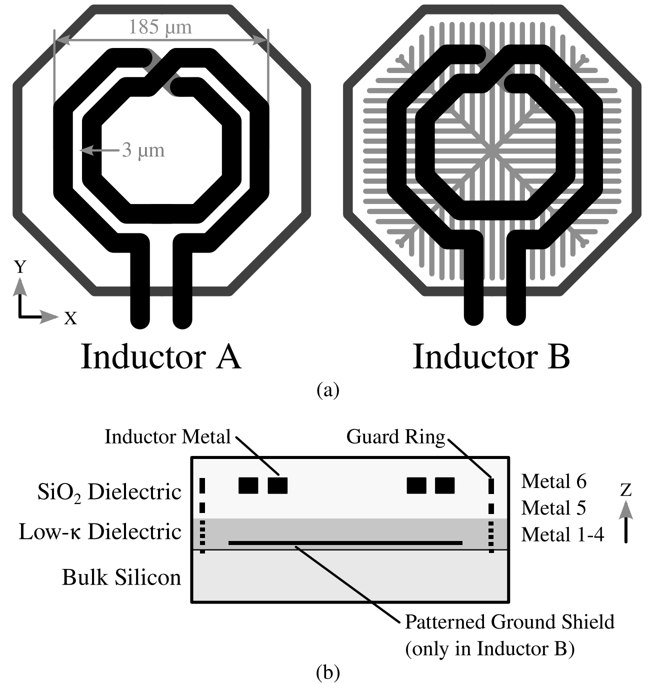

Fig. 1. (a) Comparison of inductor geometries utilized in tests. In "Inductor A," the conductor is placed directly above the silicon substrate. In "Inductor B," a patterned metal ground shield is included on the lowest metal layer above the silicon substrate. (b) Cross section of the sample technology (not to scale).

III. Experimental Methodology

Even though the circuit described above includes many circuit-level mitigation measures for known SEE sensitivities, an unforeseen radiation sensitivity was identified during a qualification test campaign. This test had revealed a single-event effect cross section exceeding 1×10^{-4} cm^2 for transient phase errors of the PLL circuit. Since this value is approximately two orders of magnitude larger than what was expected in terms of sensitive circuit area from previous experiments on similar circuits, further experiments were needed to identify the origin of this sensitivity. To gain insight into the origin and mechanism of the effect, measurement setups with sufficient resolution were developed, and multiple irradiation test campaigns were carried out. In the following, the experimental setups and the operational procedures will be described.

A. Heavy Ion Microbeam Irradiation

Selective irradiation of the circuit was performed using the GSI Heavy Ion Microbeam Facility [13] in order to localize the

origin of the SEE response inside the circuit area. In contrast to broadbeam irradiation facilities, this facility offers precise positioning capabilities for a heavy ion beam with a full-width at half-maximum (FWHM) of less than 1 μm. Conceptually, the ion beam is scanned across the circuit under test, while a data acquisition system is provided with a trigger signal whenever an SEE response of the circuit is detected by external instrumentation. In this way, a sensitivity map of the circuit under test can be created, which is then overlaid on a photomicrograph.

Using this facility, irradiation was performed using $^{40}Ar^{10+}$ ions (LET_{Si} = 10.8 MeV mg^{-1} cm^2, range exceeding 100 μm in silicon), sufficient to stimulate the responses observed in the qualification campaign. The facility accelerator operates at a fixed bunch frequency of 12.5 Hz and a particle rate of approximately 70 Hz after collimation was achieved. The circuit is scanned in a line-wise fashion at a speed of approximately 1 line/s for regions of interest spanning about 100–500 μm in each direction. Scans of the same area are performed multiple times in order to obtain a meaningful number of events for the sensitive regions. Particular care was taken to validate the relative positioning of the ion beam and the photomicrograph to within 10 μm. A dedicated SEU test structure present on the same die was used for this purpose, being placed at a known location relative to the PLL circuit.

The circuit used in this test implements “Inductor A,” which does not include a PGS. Since the device is flip-chip mounted to a carrier board, the sample was irradiated from the backside, i.e., with the particle beam incident on the bulk silicon. To reduce energy loss in the silicon, the sample was thinned to 60 μm by grinding and polishing.

During this test, the PLL circuit was operated in closed-loop mode locked to a low jitter reference clock. A trigger signal was generated whenever the output clock phase of the PLL deviated from its baseline value by more than 200 ps. An field-programmable gate array (FPGA)-based time-to-digital converter (TDC) with a time resolution of 100 ps was used for this purpose, the implementation of which is described in detail in [14]. The discriminator threshold was manually trimmed by means of a fine phase adjustment to maximize the detection sensitivity while rejecting events caused by noise. Even though the trigger threshold of this system is nominally 200 ps, its precise value is subject to an uncertainty of ±50 ps (0.5LSB).

B. Two-Photon Absorption Laser Irradiation

A two-photon absorption (TPA) laser irradiation test [15] was performed as a complementary technique to the microbeam irradiation since it also offers high spatial resolution. Conceptually, the photon energy of a single photon at wavelengths used for this test is below the energy bandgap of silicon. The electron–hole pairs (EHPs) can be generated only through nonlinear absorption of two coincident photons in the interaction region of a focused laser beam. Since this interaction region is small in both the horizontal and vertical directions, 3-D mapping of sensitive regions can be performed with this technique. A PULSCAN PULSYS irradiation system using a 540-fs pulse laser operating at a wavelength of 1550 nm was used. The laser was operated with a 1-kHz pulse repetition rate, and pulse energies up to 3 nJ have been used. During the tests, the PLL circuit operated in closed-loop mode and was instrumented using the same phase measurement system used for the microbeam test.

An important aspect of this test is its capability to stimulate the generation of EHPs only in silicon portions of integrated circuits due to differences in energy bandgap compared to dielectric materials. The 1.12-eV energy bandgap of bulk silicon is below the combined energy of two photons (two times 0.7 eV at a wavelength of 1550 nm), which is why nonlinear absorption of two coincident photons can stimulate EHP generation. Dielectric materials possess a significantly larger energy bandgap, for example, 8.9 eV in SiO_2, such that TPA and associated EHP generations do not occur in these materials at available laser wavelengths.

The circuit samples used in the Microbeam facility (containing “Inductor A” without a PGS) were reused in this test, which was carried out at the ESAT laboratory of KU Leuven. Irradiation was performed through thinned silicon dies from the backside of the circuit. Different areas of the PLL circuit were scanned in a raster-like fashion with programmable speeds, depending on the chosen pulse repetition rate. A network interface was used to signal the presence of a SEE response to the data acquisition (DAQ) system for a given position, which allows creating similar sensitivity maps as obtained through Microbeam heavy ion irradiation. The system is also equipped with a near-infrared camera system, to which the silicon substrate appears transparent. This means that the circuit’s active regions and metal layers can be imaged together with the laser interaction region, guaranteeing precise positional alignment.

C. Heavy Ion Broadbeam Irradiation

In order to further characterize the observed sensitivity, especially as a function of the used heavy ion specimen and its LET_{Si}, the circuit was irradiated with heavy ions at the Heavy Ion Facility of the Cyclotron Resource Centre, Louvain-la-Neuve, Belgium. The circuit was irradiated using six different ions, ranging in LET_{Si} from 1.3 MeV mg^{-1} cm^2 to 62.5 MeV mg^{-1} cm^2. A flux of 1.5×10^4 s^{-1} cm^{-2} was used, and a fluence of 1×10^7 cm^{-2} was collected for each ion. In order to better understand the influence of the path length of heavy ions through the sensitive geometry, irradiation of each ion was performed at three angles (0°, 35°, and 50° measured from the normal of the circuit surface).

For this test, a variant of the PLL circuit containing “Inductor B” with the previously described PGS was utilized. Since this sample utilized wire-bonding instead of being flip-chip mounted, irradiation was performed from the front side of the sample (i.e., with ions incident on the metallization layers first, before traversing the silicon). Since front side irradiation is used, no thinning of the dies has been performed.

Since the previous tests had localized the sensitive area of the circuit within the VCO, the circuit was operated in two distinct modes of operation during this test.

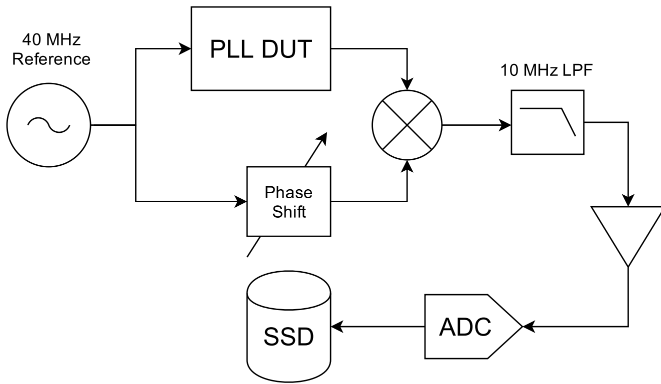

Fig. 2. High-resolution closed-loop phase measurement system.

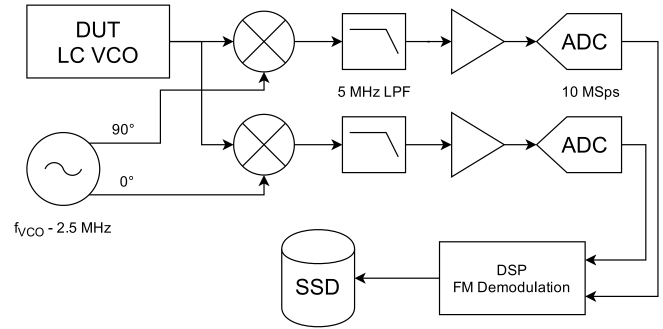

Fig. 3. High-resolution open-loop frequency measurement system used during broadbeam ion irradiation.

1) Similar to the microbeam and TPA laser tests, *closed-loop* operation was performed, during which the PLL control loop was engaged and the VCO phase-locked to an external reference clock. This mode was used to allow characterizing the impact of SEE on the in-system performance of the circuit and for comparisons with the other experiments. In this mode of operation, the PLL phase error was observed using an improved transient phase measurement system (described in the following).
2) In addition, the *open-loop* operation of the PLL circuit was performed. In this mode of operation, the feedback control was disabled, and the VCO tuning voltage was tied to a fixed voltage in the middle of its tuning range. This mode of operation was chosen for two reasons. First, it eliminates any potential contribution of SEE occurring in the reference clock path, phase detector, charge pump, and loop filter from interfering with observations. Second, it allows observing the evolution of the radiation-induced transients inside the VCO directly, without any of the feedback control loop's dynamics being superimposed. In this mode of operation, the frequency of the oscillator is measured using a precision transient frequency measurement system, which is also described in the following.

1) High-Resolution Phase Measurement Setup: The high precision transient phase measurement system used for characterization of SEE phase responses during closed-loop operation is conceptually shown in Fig. 2. In this setup, the phase difference between the two coherent clocks is measured using a linear phase detector. The operation in the linear region of the phase detector sensitivity curve is ensured by appropriately shifting the phase of the reference clock. The noise floor inherent to the measurement setup is significantly below 1-ps rms in a measurement bandwidth of 10 Hz–10 MHz. The output of this system is digitized using a sampling rate of 20 MHz. The DAQ system operates in a dead-time-free fashion and is able to store all generated data in real time to a solid-state drive. This guarantees capturing all generated events during irradiation. Event detection (triggering), classification, and data reduction tasks are performed offline. To obtain maximum sensitivity, the system noise was confirmed to be dominated by the phase noise present on the PLL output clock, which is about 2-ps rms. The event detection threshold of this experimental setup is determined solely by the total jitter of the PLL clock, not anymore by the measurement resolution, as in the previously described experiments.

2) Frequency Measurement Setup: Since the radiation-induced frequency errors in the VCO are small (on the order of parts per million), a system for obtaining high-precision frequency measurements with the very high temporal resolution was developed and is shown in Fig. 3. The VCO clock is divided by four (using the on-chip prescaler) and fed into a quadrature RF downconverter front end, which is used together with appropriate low-pass filtering to allow transient frequency measurements better than 5-ppm rms in a 5-MHz bandwidth. The frequency information is recovered by complex downconversion and frequency demodulation of the digitized baseband signal in the digital domain. The use of quadrature signal processing provides independence of the phase relationship between measurement and reference clock, allowing precise frequency measurements on a sample-by-sample basis. Again, all raw data produced during the irradiation were stored, which allows trigger processing (preprocessing and discrimination), classification, and data reduction to be performed offline. Similar to the closed-loop test setup, the noise floor of this measurement was found to be dominated by the phase noise present on the VCO clock.

IV. Measurement Results

A. Heavy Ion Microbeam Irradiation

The complete area of the PLL has been scanned using the heavy ion microbeam. Primarily, a large sensitive area was identified in the area occupied by the VCO's main spiral inductor, dominating the sensitivity. A detailed scan of only this area has been performed, and the number of detected SEE responses from the circuit are stored as a function of the beam position during the scan. The resulting sensitivity map of this process for a scan area centered on the on-chip inductor is shown in Fig. 4. The largest sensitivity appears in the vicinity of the wires forming the two inductor turns. In the center of the inductor, the sensitivity appears significantly reduced. The sensitive area highlighted in Fig. 4 was found to be approximately 4×10^{-4} cm^2. Neither the circuit area occupied by the loop filter capacitor (not visible in Fig. 4) nor any other circuit component showed any sensitivity of comparable cross section during the scans performed. The sensitive area

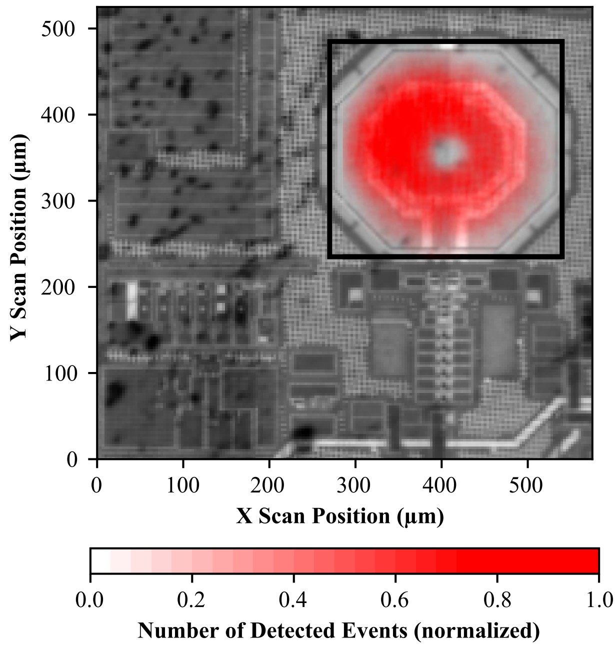

Fig. 4. Circuit sensitivity map obtained using microbeam irradiation. Color intensity encodes the number of detected responses under irradiation over multiple consecutive raster scans. The rectangular border delimits the scan extent chosen to obtain this data.

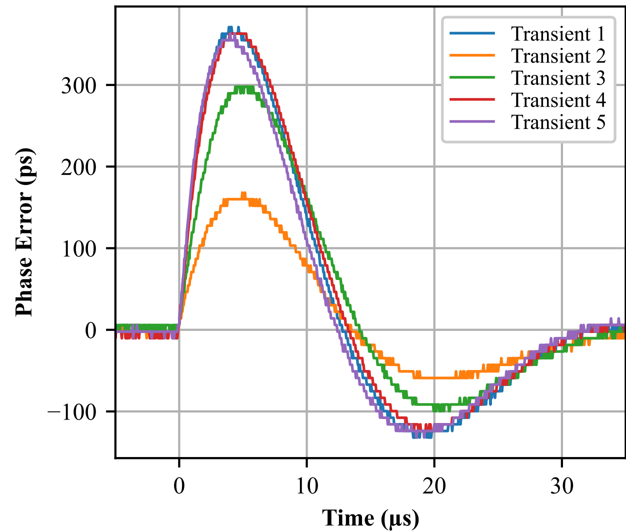

Fig. 5. Phase transients stimulated by broadbeam irradiation with $^{124}Xe^{35+}$ ions (LET_{Si} = 62.5 MeV mg^{-1} cm^2). Transients vary in peak amplitude but are very similar in temporal evolution. After the initial deviation from zero phase error up to about 5 μs, the transient shape is determined by the active PLL control.

corresponding to the spiral inductor aligns well with the cross section that the initial qualification campaign of the circuit had identified.

B. Two-Photon Absorption Laser Irradiation

The sensitive depth (Z position) of the active devices in the PLL circuit has been initially established by irradiating active devices connected to a sensitive node with a very small area (order of 1 μm) in the PLL charge pump using a pulse energy of 1.5 nJ. Following this setup procedure, selective irradiation of the area occupied by the inductor was performed. The Z position of the laser was scanned at least 10 μm in each direction to account for the possibility of a different sensitive depth. Even though these scans covered different depths in the substrate (where the laser is capable of stimulating EHP generation), they failed to stimulate any detectable responses from the circuit during irradiation of the inductor area. While the initial setup had been performed with pulse energies of about 1.5 nJ to avoid damaging MOS devices, the pulse energy was increased to 3 nJ in this area, again without being able to stimulate any responses from the circuit. Nonetheless, the full area of the PLL circuit area was scanned, but no sensitive areas of comparable cross section to the microbeam test were revealed.

C. Heavy Ion Broadbeam Irradiation

Since the previous experiment established that the SEE responses could not be reproduced with TPA laser irradiation, a broadbeam irradiation test using multiple heavy ion species was finally performed to characterize the nature of the circuit response quantitatively.

1) Closed-Loop PLL Measurements: Phase deviations of the PLL were again confirmed to be stimulated by heavy ion irradiation of various LET_{Si}. A number of representative examples of these transient responses when irradiating with $^{124}Xe^{35+}$ ions (LET_{Si} = 62.5 MeV $mg^{-1}cm^2$) are shown in Fig. 5. The shape of the responses reveal that irradiation of the sensitive area primarily results in a deviation of the VCO oscillation frequency: Instead of a step-like phase discontinuity, such a frequency disturbance results in a gradual accumulation of phase error during the first ~5 μs of the transient response. Subsequently, this accumulated error is corrected by the feedback loop with the PLL returning to its initial phase value after about 30 μs. This recovery period is entirely dominated by the PLL dynamics, not necessarily by the decay of the frequency error stimulated by irradiation. The cross section for the peak phase error exceeding different phase thresholds was calculated from the collected data and is shown in Fig. 6.

Further insight into the dependence of the ion LET_{Si} and incidence angle can be gained by looking at the distribution of the peak phase error stimulated by irradiation. The resulting distributions for three different ions and three angles are shown in Fig. 7. A number of interesting characteristics become apparent. Detectable phase excursions ($\geq$50 ps) are stimulated already for low values of LET_{Si}. For higher values of LET_{Si}, the distributions expand toward larger peak values. Also notable is the consistent expansion of the distribution toward larger peak values for shallower incident angles of heavy ions. For LET_{Si} exceeding 30 MeV mg^{-1} cm^2 (not shown in Fig. 7), the peak phase error was found not to significantly increase any further. From the shape of the distributions (which represent the variation of the peak phase error stimulated by each incident ion), it is apparent that the sensitive region does not have either homogeneous or discrete levels of sensitivity, but, instead, a continuous range of different phase errors is stimulated.

The responses shown in Fig. 5 also illustrate how the feedback control of the PLL counteracts the buildup of phase error after the oscillator frequency is disturbed by radiation.

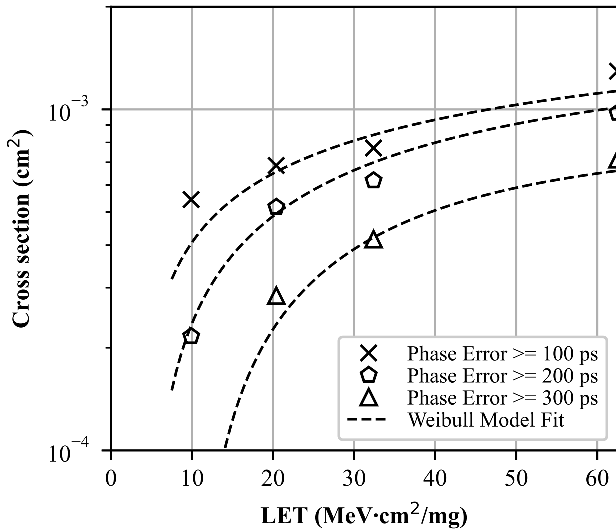

Fig. 6. Measured cross section during broadbeam heavy ion irradiation for different phase thresholds. Cross sections were obtained by counting the number of events exceeding a given phase excursion threshold for each used ion specimen. The given values are calculated for 0° ion incident angle.

Since it is, however, possible that the underlying oscillator frequency errors persist for much longer than the feedback loop response time, the following direct measurements of the oscillator frequency without PLL control feedback become crucial to understand the underlying mechanism.

2) Open-Loop VCO Measurements: Transient changes of the open-loop frequency were observed for all ion energies used in the test. Fig. 8 shows a sample of frequency transients collected with $^{124}Xe^{35+}$ and $^{36}Ar^{11+}$ ions. For both ions, the radiation response is characterized by a step-like frequency increase, which then decays back to the initial value. The temporal evolution of the generated frequency error changes significantly for LET_{Si} exceeding 10 MeV mg^{-1} cm^2. For those higher values of LET_{Si}, a sharp peak decaying in a few microseconds appears superimposed on the slow recovery process present also for lower LET_{Si}. Fig. 9 better visualizes this difference by showing the evolution of frequency error on a logarithmic time axis. Detectable residuals of the effect persist for at least 10ms after stimulation of the response, with the effect approaching full decay only at around 100ms. For LET_{Si} exceeding 10 MeV mg^{-1} cm^2, the frequency error may exceed 50 ppm for up to 100 μs.

Similar to the analysis performed for the stimulated phase error in the closed-loop PLL measurements, the distribution of peak frequency errors generated by irradiating the sensitive area can be computed. The distributions produced by two different ions are shown in Fig. 10. In agreement with the measurements obtained for the closed-loop operation, higher particle LET_{Si} results in larger peak errors being stimulated. Also notable is the continuous distribution of peak frequency errors, which indicates a nonhomogeneous sensitivity of the geometry.

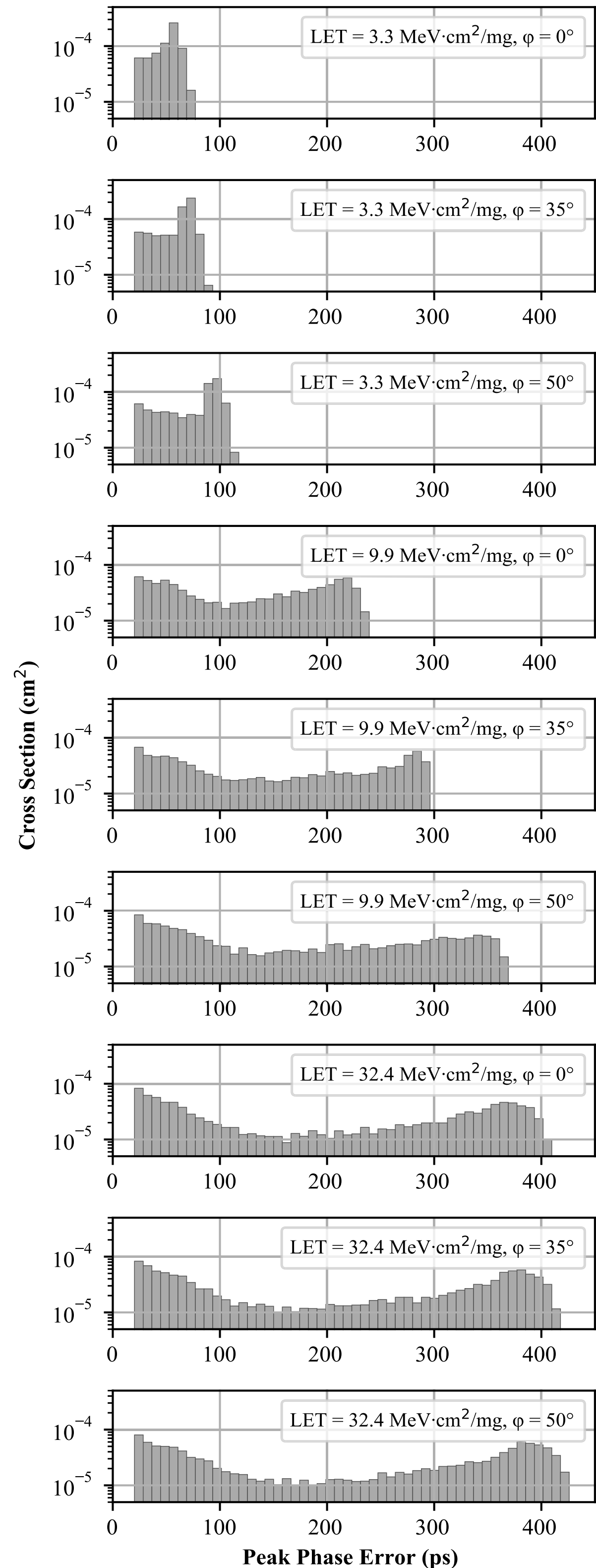

Fig. 7. Distribution of the peak clock phase error stimulated by heavy ion irradiation. A consistent expansion of the phase error distribution is observed with higher LET_{Si} and shallower particle incident angles.

V. Discussion of Measurement Results

A. Contribution of Pileup

Pileup was a concern in both heavy ion irradiation experiments performed. A particularity of the microbeam facility is the operation at a low bunch frequency of 12.5 Hz. While the collimation used to achieve the small beamwidth reduces the rate of particles on the tested sample significantly, around

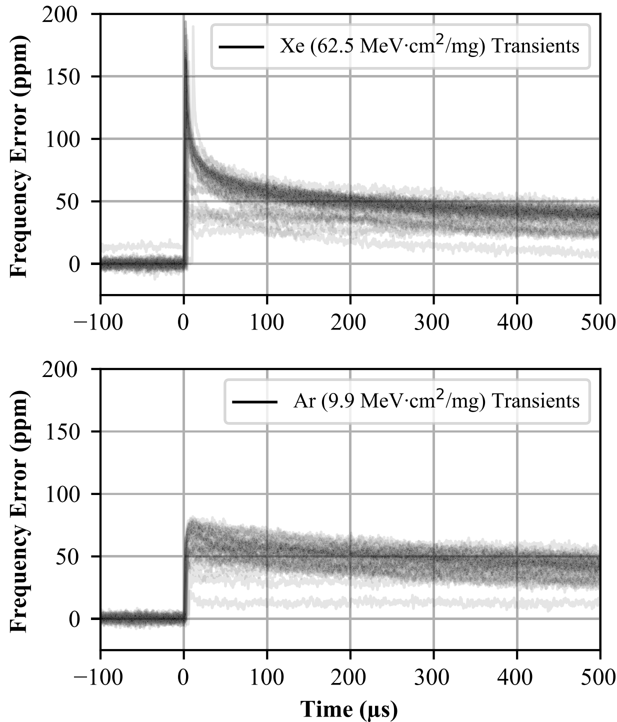

Fig. 8. Frequency transients stimulated during broadbeam heavy ion irradiation. The response to irradiation with $^{124}Xe^{35+}$ ions is characterized by a pronounced initial frequency step, which quickly decays. This initial response is not observed with $^{36}Ar^{11+}$ ions.

70 ions arrive at the sample surface per second. This means that each bunch delivers about five ions to a given position of the microbeam. As a result, the circuit responses used for Fig. 4 are the result of multiple simultaneous ion hits. Since no quantitative information about pulse height or transient duration was obtained during the microbeam experiment, the only impact on this experiment is an increase in the detection sensitivity.

In the broadbeam irradiation experiments, the combination of a high ion flux with the long persistence of the radiation effect was observed to occasionally result in a pileup. This manifested as a baseline shift of recorded transients, as a result of a previous radiation response not having fully decayed. Since raw transient data were recorded, this problem could be remedied by using the baseline frequency as an additional qualifier during off-line trigger processing. This procedure very efficiently discarded these events, and since the proportion of events affected by pileup was found to be low, their removal has little influence on the reported cross sections.

B. Microbeam Scan Artifacts

The second issue affecting the data shown in Fig. 4 is the approach adopted for scanning the circuit area. The circuit is scanned in a linewise fashion at a low speed of ∼1 line/s. The facility accelerator operates independently of this scan frequency at a bunch frequency of 12.5 Hz. The bunched irradiation, therefore, constitutes a spatial sampling process, and not all positions along the scan lines are covered with equal density. Since the line frequency and the accelerator bunch frequency are not relative multiples, artifacts, such as diagonal lines of increased or reduced sensitivity, appear in the resulting sensitivity maps. These artifacts change when modifying the scan frequency, which complicates comparisons of measurements obtained with different scan rates and beam deflections. One feature affected by this issue is the "hole" in the center of the inductor geometry, which did not show the same reduction of sensitivity in all the scans performed. To mitigate scanning artifacts, the collected data are rebinned or low-pass filtered. This process sacrifices resolution and may distort the shape of the sensitive area depending on the bin width or filter kernel. As a consequence of these limitations, no attempts were made to extract quantitative information other than the location and area of the sensitive circuit component from the sensitivity map.

C. Correspondence Between Microbeam and Broadbeam Heavy Ion Irradiations

The microbeam experiment was used to confidently constrain the position of the sensitive area inside the circuit and to obtain an estimate for its size. It also confirmed that this single sensitive area by far dominates the sensitivity of the circuit. Since this experiment utilized a rather coarse-grained phase measurement setup, which could only be used for detection (instead of precisely measuring the amplitude) of the SEE events, the sensitivity map obtained allows only limited interpretation of the results. It clearly reveals, however, that the area occupied by the on-chip spiral inductor is not homogeneously sensitive to irradiation since the number of detected events is not constant across its area. These conclusions are fully supported by the broadbeam heavy ion irradiation experiments. Comparing the sensitive circuit area estimate from the microbeam experiments (4×10^{-4} cm^2) with the data point in Fig. 6 taken at comparable detection threshold and LET_{Si} (2×10^{-4} cm^2 for a threshold of 200 ps and LET_{Si} of 10 MeV mg^{-1} cm^2), the two figures are found to be in very good agreement. Also, the nonhomogeneous sensitivity of the area shown in Fig. 4 is consistent with the obtained distributions of peak phase errors shown in Fig. 7. The broadbeam measurements showed that irradiation of random points inside the sensitive area creates a continuum of peak phase error magnitudes. This behavior is reflected also in the magnitude distribution of the underlying frequency errors that were found to follow a similarly continuous distribution (see Fig. 10). The transport of ions in matter (TRIM) [16] code was used to confirm that the LET in the SiO_2 layers was comparable for both experiments using argon ions available at both facilities such that comparisons between frontside and backside irradiations remain valid.

D. Role of Silicon and Dielectric Layers

While the interactions of heavy ions with active devices in silicon integrated circuits are a very widely studied topic, no active devices are present in the sensitive area that could explain such sensitivity. Of particularly surprising nature is the long decay time of the effect, which was found experimentally

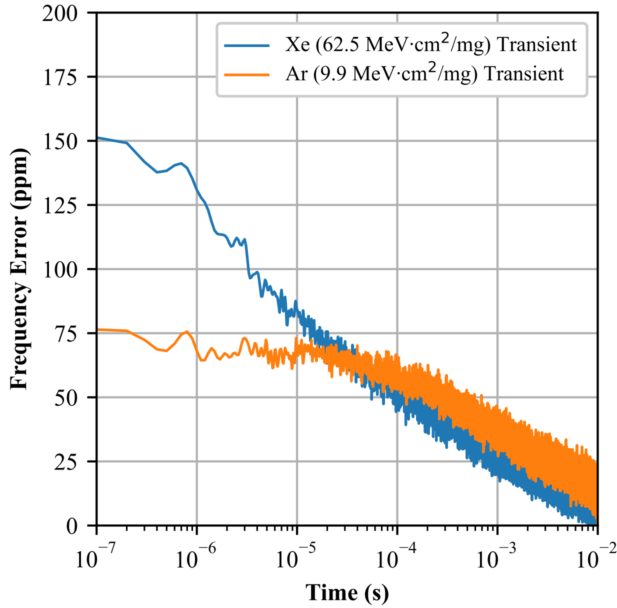

Fig. 9. Frequency transients stimulated by broadbeam heavy ion irradiation shown on a logarithmic time scale. Detectable residuals of frequency errors were observed to consistently persist into the millisecond timescale.

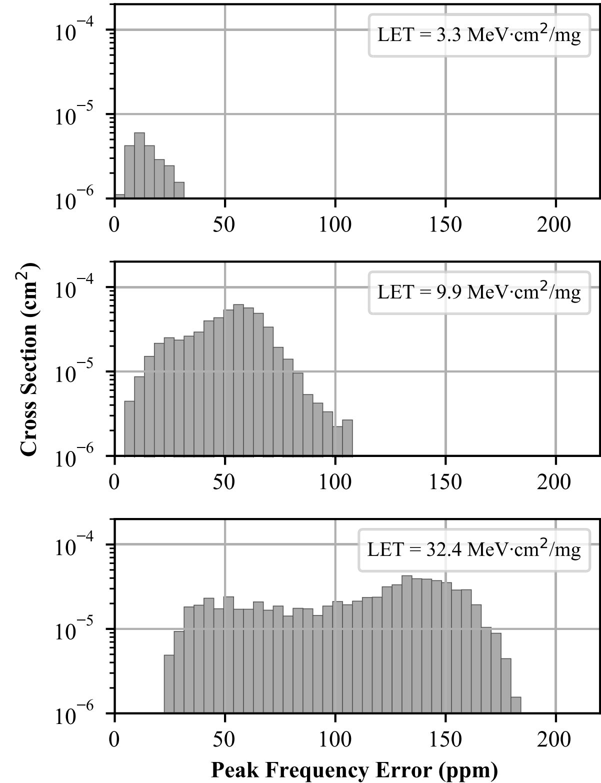

Fig. 10. Distributions of the peak oscillator frequency error stimulated by broadbeam heavy ion irradiation. A broad distribution of values is stimulated, which expands with increased particle LET_{Si}.

to extend into in the millisecond range, as highlighted in Fig. 9. Studies concerned with the interactions of heavy ions in silicon devices, such as [17], make clear that the large charge carrier densities present after ion impact persist for only fractions of nanoseconds, fully reverting to their preirradiation value within 10 ns. This makes an explanation of the observed effect involving the generated charge carriers in the silicon substrate implausible. This conclusion is supported by the fact that the PGS included in “Inductor B” (used during the broadbeam experiment) failed to result in a significant reduction of the sensitivity compared to “Inductor A” (used during the microbeam experiment). The responses seen from “Inductor B” would have been expected to be much smaller if the responsible mechanism takes place in the silicon substrate and is, therefore, shielded from the inductor by the PGS. Even though the differences in experimental setup used in the two tests do not allow precisely quantifying the difference, it can be said that the stimulated responses did have approximately the same magnitude at comparable values of LET.

Another strong indication for an origin in the dielectric layers is the absence of any circuit responses in the laser TPA experiments. Even though the used pulse energies of 3 nJ produce localized EHP densities in silicon comparable to heavy ions with an LET_{Si} of 50 MeV mg^{-1} cm^2, our experiments failed to detect any phase deviations when irradiating the bulk silicon below the inductor. As already stated in Section III, laser experiments are unable to stimulate EHP generation in the dielectric layers due to their significantly larger energy bandgap (9.3 eV for SiO_2 [18]). Heavy ions in the energy regime used in our tests, on the other hand, possess sufficient stopping power for generation of large densities of EHPs in both Si and dielectrics, such as SiO_2. These experimental findings lead us to the conclusion that the responsible mechanism is to be found in the dielectric layers above the silicon substrate.

E. Electrical Properties of Inductor Geometry

In order to propose a mechanism responsible for the generated frequency errors during irradiation of the spiral inductor, the geometry of the inductor needs to be reviewed in more detail. The planar CMOS inductor used in the structure contains notable geometric features that require appropriate electrical modeling: The small gap between both windings and their proximity to the silicon substrate in combination with the large area covered by the conductors results in large distributed parasitic capacitance of two types: first, between the two closely spaced conductors (winding-to-winding capacitance); second, between the conductors and the substrate (winding-to-substrate capacitance). At operating frequencies in the GHz range, this implies that the impedance at the inductor terminals is determined by both the inductive components and these parasitic capacitances, which shunts sections of the conductor to either the substrate or other areas of the conductor in adjacent windings. While the overall complex impedance of the structure is, indeed, inductive, the distributed capacitances (and, therefore, the dielectric properties of the surrounding materials) play a major role in determining its components.

F. Proposed Mechanism for Stimulation of Frequency Errors

Since the LET of the heavy ion species used in our experiments is very similar when considering the Si substrate

and the SiO_2 dielectrics as targets, dense tracks of free charge carriers will be created in the dielectric layers surrounding the inductor. The dielectric properties of these layers are determined by their electric polarizability. The presence of free charge carriers and potentially also the excitation of defects through ionization could result in significant changes to the local polarizability of the material, and this may locally alter its complex permittivity. We, therefore, propose that the complex impedance of the inductor structure is altered as a result of this interaction until these effects subside. This would imply either the recombination, trapping, or collection of generated carriers and the return of electrically excited defects to their initial state. Conclusive quantitative analysis of this hypothesis is unfortunately difficult for multiple reasons. One major obstacle is uncertainty about the dielectric materials and their properties in the CMOS process used in our experiments. Even when assuming that SiO_2 is used in the majority of interlevel dielectrics, the properties of SiO_2 can vary strongly depending on the chosen method of fabrication. Deposited oxide layers, for example, using CVD techniques, are typically characterized by much higher defect concentrations than thermally grown ones. These defects result in changes of quantities relevant to the polarizability, such as the charge carrier mobility and their lifetime. While the effective mobility accounts for the amount of polarizability change by a given number of free carriers, the carrier lifetime would need to be large enough to explain the experimentally observed timescales. Unfortunately, a large body of fundamental research on these properties of amorphous SiO_2 (e.g., [19] and [20]) uses thermally grown, high purity SiO_2. Free electrons in this type of SiO_2 possess very high mobility, which makes them contribute strongly to the change of polarizability; however, they are also characterized by very short lifetimes (on the order of tens of nanoseconds) [19]. Holes, on the other hand, are shown to have much lower mobility but significantly greater lifetimes. The lifetime of holes in amorphous SiO_2 was reported to exceed 100ms at room temperature [20]. Another consideration here is the electrical excitation of defects in the SiO_2 and their impact on polarizability. While the literature on defects in SiO_2 indicates the presence of such excited states with decay times in the 10-ms range [21], their contribution to changes of the dielectric properties of the material remains to be quantified. Further modeling of the ionization and displacement processes in the dielectrics is required to conclusively attribute the effect to postirradiation mechanisms inside the dielectric layers. In addition, different experimental techniques must be considered to better separate different mechanisms, for example, using X-ray or deep ultraviolet radiation.

G. Sensitivity of Radiation Response to Irradiation Angle

The proposed mechanism also offers an explanation for the increase in sensitivity observed with shallower particle incident angles in the broadbeam experiments (compare Fig. 7 and Fig. 10). Even though a large surface area is sensitive to irradiation, the sensitive dielectric volume extends vertically only about 5 μm. Shallower incident angles, therefore, significantly increase the path length of individual ions through the sensitive material, which results in the generation of more free carriers along their path. Since we propose the concentration of free charge carriers or the excitation of defects to determine the magnitude of the effect, these observations are consistent with our hypothesis.

H. Relevance of Circuit Time Constants

A concern that needs to be considered is whether the long persistence time of the observed responses could be explained through time constants present in the circuit itself. Since the experiment had conclusively shown that the effect is stimulated in the VCO, the number of circuit components in which such a time constant would need to be identified is limited. It is clear that neither the primary time constant formed by the LC tank (which resonates at 5.12 GHz) nor the bandwidth of the frequency control input of the VCO can be responsible for this effect. The latter, while limited through the use of the modified varactor topology, is still in the order of 20 MHz and, therefore, may only introduce a time constant of the order of nanoseconds. One alternative hypothesis considered is shown here but was ultimately determined to be insufficient to explain the response time constants.

CMOS VCOs are known to be susceptible to AM-to-FM conversion, for example, as a result of nonlinear capacitances in the tank [1]. Long time constants on the oscillation frequency could result, while the steady-state oscillation amplitude is established through the following mechanism: Following a disturbance of the amplitude, the tank voltage envelope (which may convert into a frequency error) can be described by the exponential given in the following equation:

$$\hat{v}_{\text{tank}}(t) = e^{-\frac{t(1-g_m R)}{RC}}. \quad (1)$$

In this expression, C and R model the tank capacitance and its loss resistance, while g_m represents the transconductance of the active device. As the oscillation amplitude grows, g_m decreases as it nonlinear operation is approached, until the product $g_m R$ is unity. This fact makes g_m a function of $\hat{v}_{\text{tank}}$. Due to this relationship, the term $(1 - g_m R)$ slowly approaches zero as the amplitude grows, which, in principle, leads to an infinitely long time constant for establishing the steady-state oscillation amplitude. However, we have found that, for practical circuits, this is without significance compared to the observed responses, and this theoretically infinite time constant does not practically impact circuit operation. Both in simulations and laboratory experiments, any appreciable transient response of the tank voltage envelope following a step change vanished within a few oscillation periods, and no frequency error could be resolved after this time. We, therefore, conclude that the observed response cannot be explained by time constants inherent to the circuit.

I. Novelty of the Observation

Given that SEEs in PLL circuits have been a focus of research since many years and methods for their characterization have been reported in the scientific literature for at least 25 years [22], an explanation for discovering

the described effect only recently needs to be provided. We conclude that this is a result of at least three separate factors:

1) Dominance of Ring Oscillators in Relevant Studies: A survey of available publications concerned with the assessment of single-event effects hardness of PLL and VCO circuits revealed that the overwhelming majority of studies utilize ring oscillator VCOs. Apart from publications of our own research group, irradiation experiments performed with LC oscillators are reported in [5] and [23]–[27]. Common to all these publications is the exclusive use of laser irradiation techniques for experimental validation. While Zhang *et al.* [23] report on sensitivity in the area occupied by the inductor, the sensitivity is attributed to the tuning varactors placed in the same area. The authors specifically refer to the charge collection sensitivity of MOS varactors previously reported in [10], which cannot explain our observation. The remaining literature utilizes a single photon absorption technique and reports sensitivities only during irradiation of the active devices present in the LC oscillator. As previously explained, we hypothesize that the circuit responses that we describe do not originate in the silicon substrate. Both single- and two-photon absorption laser experiments are, however, unable to stimulate EHP generation in the dielectric layers with their larger energy bandgap.

2) Chosen PLL Bandwidth: A contributing factor influencing the magnitude of the observed radiation response is the choice of PLL bandwidth. Since the underlying radiation response was found to be a frequency error (as opposed to a phase error), the amount of phase error accumulated in the PLL is strongly dependent on the loop bandwidth. Higher loop bandwidths will result in a faster reaction of the control loop and, therefore, the accumulation of less phase error. As an example, even though the same VCO as described in this article is also used in [11], it is embedded in a high-speed CDR loop with a bandwidth of 2 MHz, a factor of 20 higher than in this work. Even though heavy ion irradiation will have stimulated the same frequency errors in this VCO, the resulting phase errors were small enough to remain below the detection threshold.

3) Detection and Measurement Sensitivity: The final contributor is the use of test equipment with sufficient sensitivity. While our group has tested low-bandwidth LC PLL circuits before, for example, in [1], transient phase instrumentation resolution in these experiments has been far lower than with the techniques applied in this work. While, in the previous work, the resolution and detection threshold of phase transients were limited to 390 ps, the detection threshold of the setup used in this work is essentially only limited by the clock jitter of the PLL itself, which is below 50-ps peak-to-peak. Other works, such as [23]–[25], utilize spectral analysis methods for the detection of phase or frequency errors instead of time-domain measurements. The achievable resolution and noise floor of these methods are not trivial to assess, but available information in these publications indicates that detection of effects on the level that we report might have been impossible in the first place due to insufficient sensitivity.

VI. Conclusion

A previously unreported radiation response affecting inductors manufactured in a commercial 65-nm CMOS process was presented. In a tested PLL circuit, the effect was shown to produce frequency errors resulting in phase excursions large enough to significantly impair circuit performance in applications requiring phase stability in the picosecond range, such as timing detectors used in high energy physics [28], [29] or communication circuits for space applications, depending on the chosen loop bandwidth. The fact that this effect was found to directly impact the performance of a low-jitter PLL circuit underlines the increasing importance of considering SEE in passive circuit components that have been traditionally assumed to be insensitive to SEE compared to their active counterparts. Multiple experiments were performed to conclusively attribute the observed sensitivity to the inductor used in the LC tank of an oscillator and quantitatively characterize the produced effect. Different hypotheses for the underlying mechanism have been discussed, and the experimental results strongly suggest that the observed responses are a result of temporarily altered polarizability of the dielectric materials surrounding the wires forming the inductor. The resulting stimulated change of the complex permittivity is assumed to alter the impedance of the inductor structure, which, in turn, changes the resonant frequency of the oscillator. Direct measurements have shown that this effect persists on timescales exceeding the 10-ms range, likely as a result of high carrier lifetime or excitation of defects in the dielectric materials. While a full quantitative treatment of the observed responses and their underlying mechanism cannot yet be provided, we suggest both further experiments and modeling approaches to better understand the origins of the effect, which will be necessary foundations for developing effective mitigation strategies for circuits using on-chip inductors (and RF and mm-wave circuits in general) in radiation environments.

Acknowledgment

The authors express their gratitude toward GSI Helmholtzzentrum für Schwerionenforschung for providing access to its Microbeam Irradiation Facility. In particular, they want to acknowledge Kay-Obbe Voss who provided them with valuable technical and operational support during the experiments in the facility.

References

[1] J. Prinzie, J. Christiansen, P. Moreira, M. Steyaert, and P. Leroux, "Comparison of a 65 nm CMOS ring- and LC-oscillator based PLL in terms of TID and SEU sensitivity," *IEEE Trans. Nucl. Sci.*, vol. 64, no. 1, pp. 245–252, Jan. 2017.

[2] J. Prinzie and V. De Smedt, "Time-dependent single-event effects in CMOS *LC*-oscillators," *IEEE Trans. Nucl. Sci.*, vol. 66, no. 9, pp. 2048–2054, Sep. 2019.

[3] Y. Gao, J. Lou, J. Zhang, L. Li, and F. Xu, "Single-event transients in LC-tank VCO," in *Proc. Int. Workshop Microw. Millim. Wave Circuits Syst. Technol.*, 2012, pp. 1–4.

[4] Z. Zhang, L. Chen, and H. Djahanshahi, "A hardened-by-design technique for LC-tank voltage controlled oscillator," in *Proc. IEEE Can. Conf. Electr. Comput. Eng. (CCECE)*, May 2018, pp. 425–427.

[5] T. Wang, K. Wang, L. Chen, A. Dinh, B. Bhuva, and R. Shuler, "A RHBD LC-tank oscillator design tolerant to single-event transients," *IEEE Trans. Nucl. Sci.*, vol. 57, no. 6, pp. 3620–3625, Dec. 2010.

[6] S. Jagannathan *et al.*, "Sensitivity of high-frequency RF circuits to total ionizing dose degradation," *IEEE Trans. Nucl. Sci.*, vol. 60, no. 6, pp. 4498–4504, Dec. 2013.

[7] T. D. Loveless *et al.*, "Combined effects of total ionizing dose and temperature on a *k*-band quadrature LC-tank VCO in a 32 nm CMOS SOI technology," *IEEE Trans. Nucl. Sci.*, vol. 64, no. 1, pp. 204–211, Jan. 2017.

[8] R. Xu *et al.*, "Single-event upset responses of metal–oxide–metal capacitors and diodes used in bulk 65-nm CMOS analog circuits," *IEEE Trans. Nucl. Sci.*, vol. 67, no. 4, pp. 698–707, Apr. 2020.

[9] S. Biereigel *et al.*, "The lpGBT PLL and CDR architecture, performance and SEE robustness," in *Proc. PoS*, 2020, p. 34.

[10] J. Prinzie, J. Christiansen, P. Moreira, M. Steyaert, and P. Leroux, "A 2.56-GHz SEU radiation hard LC-tank VCO for high-speed communication links in 65-nm CMOS technology," *IEEE Trans. Nucl. Sci.*, vol. 65, no. 1, pp. 407–412, Jan. 2018.

[11] S. Biereigel *et al.*, "A low noise fault tolerant radiation hardened 2.56 Gbps clock-data recovery circuit with high speed feed forward correction in 65 nm CMOS," *IEEE Trans. Circuits Syst. I, Reg. Papers*, vol. 67, no. 5, pp. 1438–1446, May 2020.

[12] C. P. Yue and S. S. Wong, "On-chip spiral inductors with patterned ground shields for Si-based RF ICs," *IEEE J. Solid-State Circuits*, vol. 33, no. 5, pp. 743–752, May 1998.

[13] P. Barberet, M. Heiss, G. Du, B. E. Fischer, and G. Taucher-Scholz, "The GSI heavy ion microbeam: A tool for the investigation of cellular response to high LET radiations," *Acta Phys. Polonica A*, vol. 10950, pp. 329–334, Mar. 2006.

[14] S. Biereigel, S. Kulis, P. Moreira, J. Prinzie, P. Leroux, and A. Koelpin, "Methods for clock signal characterization using FPGA resources," *J. Instrum.*, vol. 15, no. 3, Mar. 2020, Art. no. P03012.

[15] D. McMorrow, W. T. Lotshaw, J. S. Melinger, S. Buchner, and R. L. Pease, "Subbandgap laser-induced single event effects: Carrier generation via two-photon absorption," *IEEE Trans. Nucl. Sci.*, vol. 49, no. 6, pp. 3002–3008, Dec. 2002.

[16] J. F. Ziegler, M. D. Ziegler, and J. P. Biersack, "SRIM—The stopping and range of ions in matter (2010)," *Nucl. Instrum. Methods Phys. Res. B, Beam Interact. Mater. At.*, vol. 268, nos. 11–12, pp. 1818–1823, Jun. 2010. [Online]. Available: https://www.sciencedirect.com/science/article/pii/S0168583X10001862

[17] L. Artola, G. Hubert, S. Duzellier, and F. Bezerra, "Collected charge analysis for a new transient model by TCAD simulation in 90 nm technology," *IEEE Trans. Nucl. Sci.*, vol. 57, no. 4, pp. 1869–1875, Aug. 2010.

[18] Z. A. Weinberg, G. W. Rubloff, and E. Bassous, "Transmission, photoconductivity, and the experimental band gap of thermally grown SiO_2 films," *Phys. Rev. B, Condens. Matter*, vol. 19, no. 6, p. 3107, Mar. 1979.

[19] R. C. Hughes, "Charge-carrier transport phenomena in amorphous SiO_2: Direct measurement of the drift mobility and lifetime," *Phys. Rev. Lett.*, vol. 30, p. 1333, Jun. 1973, doi: 10.1103/PhysRevLett.30.1333.

[20] R. C. Hughes, "Hole mobility and transport in thin SiO_2 films," *Appl. Phys. Lett.*, vol. 26, no. 8, pp. 436–438, 1975.

[21] L. Skuja, "Optically active oxygen-deficiency-related centers in amorphous silicon dioxide," *J. Non-Cryst. Solids*, vol. 239, nos. 1–3, pp. 16–48, Oct. 1998. [Online]. Available: https://www.sciencedirect.com/science/article/pii/S0022309398007200

[22] K. Jobe, M. Shoga, and R. Koga, "A systems-oriented single event effects test approach for high speed digital phase-locked loops," *IEEE Trans. Nucl. Sci.*, vol. 43, no. 6, pp. 2868–2873, Dec. 1996.

[23] Z. Zhang, H. Djahanshahi, C. Gu, M. Patel, and L. Chen, "Single-event effects characterization of LC-VCO PLLs in a 28-nm CMOS technology," *IEEE Trans. Nucl. Sci.*, vol. 67, no. 9, pp. 2042–2050, Sep. 2020.

[24] S. Guo, J. Li, P. Gui, Y. Ren, L. Chen, and B. L. Bhuva, "Single-event transient effect on a self-biased ring-oscillator PLL and an LC PLL fabricated in SOS technology," *IEEE Trans. Nucl. Sci.*, vol. 60, no. 6, pp. 4668–4672, Dec. 2013.

[25] S. Jagtap, S. Anmadwar, S. Rudrapati, and S. Gupta, "A single-event transient-tolerant high-frequency CMOS quadrature phase oscillator," *IEEE Trans. Nucl. Sci.*, vol. 66, no. 9, pp. 2072–2079, Sep. 2019.

[26] W. Chen *et al.*, "Impact of VCO topology on SET induced frequency response," *IEEE Trans. Nucl. Sci.*, vol. 54, no. 6, pp. 2500–2505, Dec. 2007.

[27] W. Chen *et al.*, "Investigation of single-event transients in voltage-controlled oscillators," *IEEE Trans. Nucl. Sci.*, vol. 50, no. 6,pp. 2081–2087, Dec. 2003.

[28] ATLAS Collaboration, "Technical design report: A high-granularity timing detector for the ATLAS phase-II upgrade," CERN, Geneva, Switzerland, Tech. Rep. CERN-LHCC-2020-007 and ATLAS-TDR-031, Jun. 2020. [Online]. Available: https://cds.cern.ch/record/2719855 and https://cds.cern.ch/record/2719855/files/ATLAS-TDR-031.pdf

[29] CMS Collaboration, "A MIP timing detector for the CMS phase-2 upgrade," CERN, Geneva, Switzerland, Tech. Rep. CERN-LHCC-2019-003 and CMS-TDR-020, Mar. 2019. [Online]. Available: https://cds.cern.ch/record/2667167 and https://cds.cern.ch/record/2667167/files/CMS-TDR-020.pdf